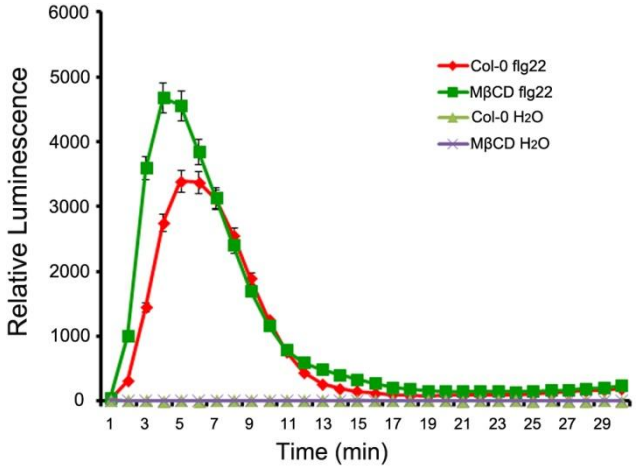

Fig. S1. MβCD affected flg22-induced ROS production.

In time-course experiments, ROS production was elevated under flg22 and MβCD co-treatment compared to flg22 treatment (Values are means ± SDs; n $\geqslant$ 4; three biological repeats).

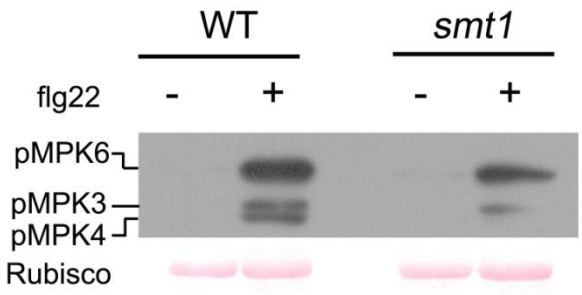

Fig. S2. Detection of the MAPKs phosphorylation in *Arabidopsis thaliana* in response to flg22 in WT and *smt1* mutants. No phosphorylated MAPKs were detected in the untreated sample (-).

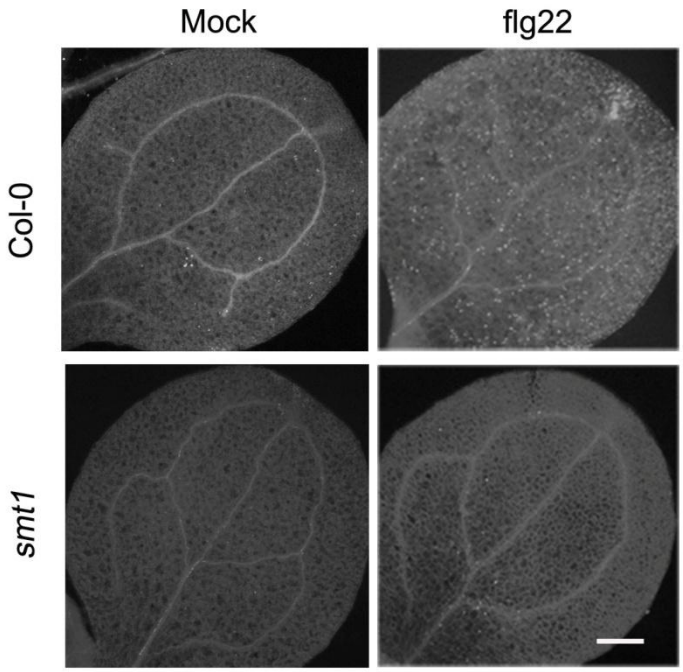

Fig. S3. Flg22 induced callose deposition.

Callose deposition in 2-week-old leaf tissue of the WT and the *smt1* mutants at 24 hr after infiltration with flg22. Representative images are shown depicting differences in callose deposition between Col-0 and *smt1* mutants under mock and flg22 treatments. Scale bar = 0.5 mm (Untreated, n = 9 images; flg22 treated, n = 12 images from two biological replicates).

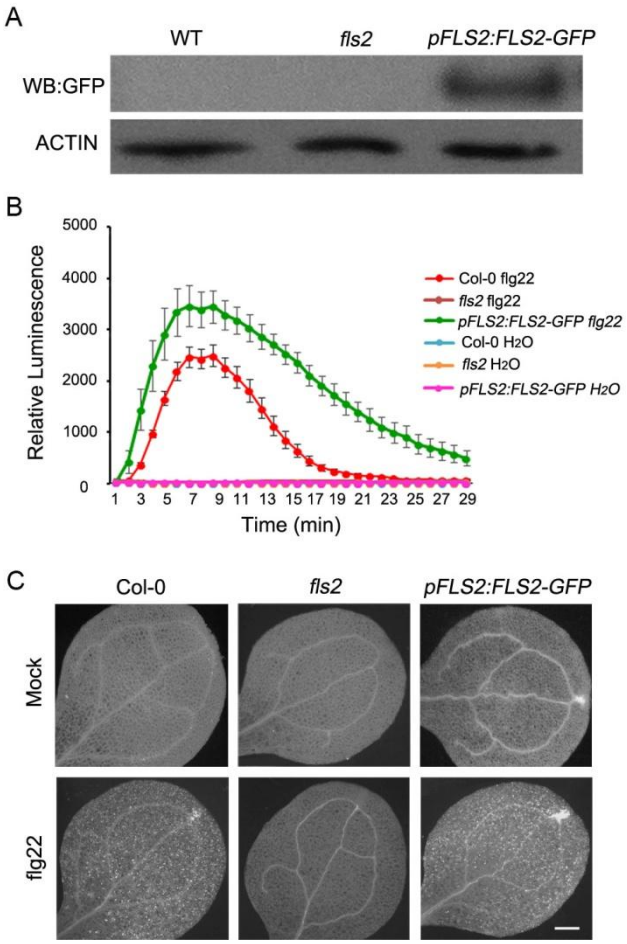

Fig. S4. Rescue of the *fls2* mutant by a genomic sequence of *FLS2* fused with the *GFP* sequence in *Arabidopsis* leaves.

(A) Immunoblot analysis of total protein extracts from WT, *fls2* (as a control) and FLS2-GFP transgenic *Arabidopsis* seedlings probed with GFP and ACTIN antibodies.

(B) Flg22-triggered (100 nM) ROS burst in Col-0, *fls2*, and pFLS2:FLS2-GFP transgenic seedlings. (Values are means ± SDs; n ⩾ 4; two biological repeats)

(C) Measurement of callose deposition in Col-0, *fls2*, and pFLS2:FLS2-GFP transgenic seedlings using aniline blue staining under mock or 2 μM flg22 treatment for 24 h. Bar =200 μm. (Untreated, n = 9 images; flg22 treated, n = 17 images pooled from two biological replicates)

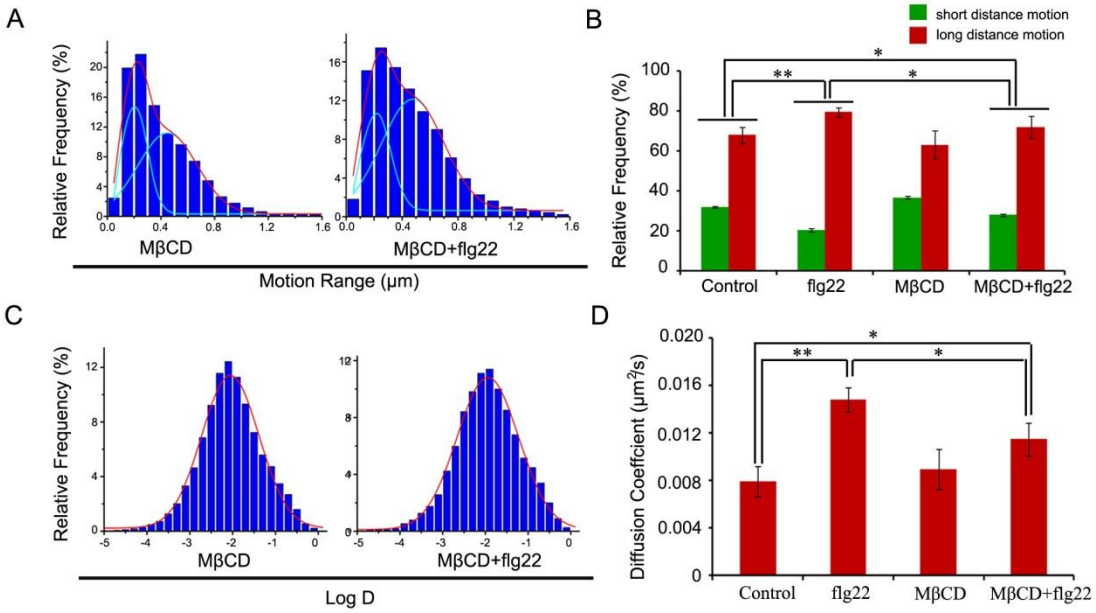

Fig. S5. Effects of MβCD treatment on the dynamic behavior of FLS2-GFP.

(A) Distribution of motion ranges of FLS2-GFP spots under MβCD (n = 10811 spots), MβCD and flg22 co-treatment (n = 7738 spots), respectively.

(B) Frequency of long distance and short distance motions for FLS2-GFP under different treatments. Error bars represent the SD. Statistical significance was checked by Student's *t*-test (*P <0.05).

(C) Distribution of diffusion coefficients of FLS2-GFP spots under MβCD (n = 12592 spots), MβCD and flg22 co-treatment (n = 9610 spots), respectively.

(D) Diffusion coefficients of FLS2-GFP spots under different treatments. Error bars represent the SD. Statistical significance was checked by Student's *t*-test (*P <0.05 and **P < 0.01).

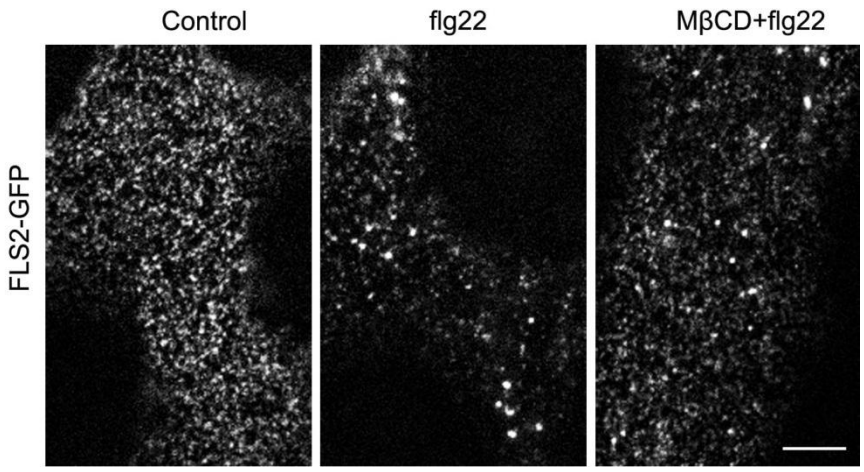

Fig. S6. Typical images showing diffraction-limited fluorescent spots of FLS2-GFP on a fixed cell membrane of *Arabidopsis* leaf epidermal cells under flg22 treatment and co-treatment with MβCD and flg22, imaged with TIRFM. The image is a section of the first frame of a stack of images with the background subtracted (Scale bar: 1 µm).

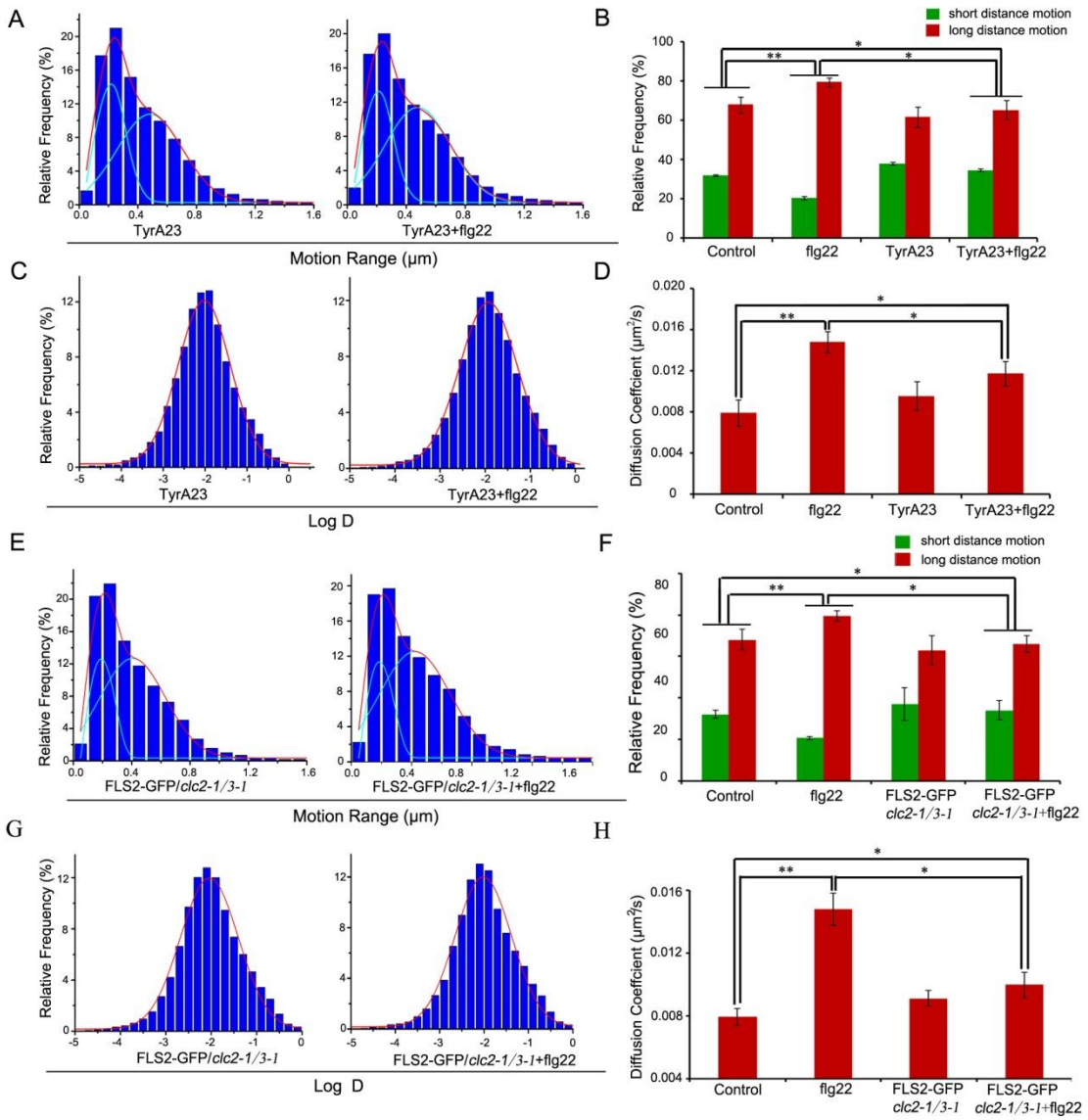

Fig. S7. Clathrin is required for FLS2 dynamics.

(A) Distribution of FLS2-GFP motion range under TyrA23 treatment (n = 14401 spots), TyrA23 and flg22 co-treatment (n = 11445 spots).

(B) Frequency of long distance and short distance motions for FLS2-GFP under different treatments. Error bars represent the SD. Statistical significance was checked by Student's *t*-test (*P <0.05 and **P < 0.01).

(C) Distribution of FLS2-GFP diffusion coefficients under TyrA23 treatment (n = 17147 spots), TyrA23 and flg22 co-treatment (n = 28319 spots).

(D) Diffusion coefficients of FLS2-GFP under different treatments. Error bars represent the SD. Statistical significance was checked by Student's *t*-test (*P <0.05 and **P < 0.01).

(E) Distribution of FLS2-GFP motion range in *clc2-1 clc3-1* mutant (n = 9870 spots) and in *clc2-1 clc3-1* mutant seedlings after flg22 (n = 11342 spots).

(F) Frequency of long distance and short distance motions for FLS2-GFP in *clc2-1 clc3-1* mutant. Error bars represent the SD. Statistical significance was checked by Student's *t*-test (*P <0.05 and **P < 0.01).

(G) Distribution of FLS2-GFP diffusion coefficients in *clc2-1 clc3-1* mutant (n = 9311 spots) and in *clc2-1 clc3-1* mutant seedlings after flg22 (n = 12776 spots).

(H) Diffusion coefficients of FLS2-GFP in *clc2-1 clc3-1* mutant. Error bars represent the SD. Statistical significance was checked by Student's *t*-test (*P <0.05 and **P < 0.01).

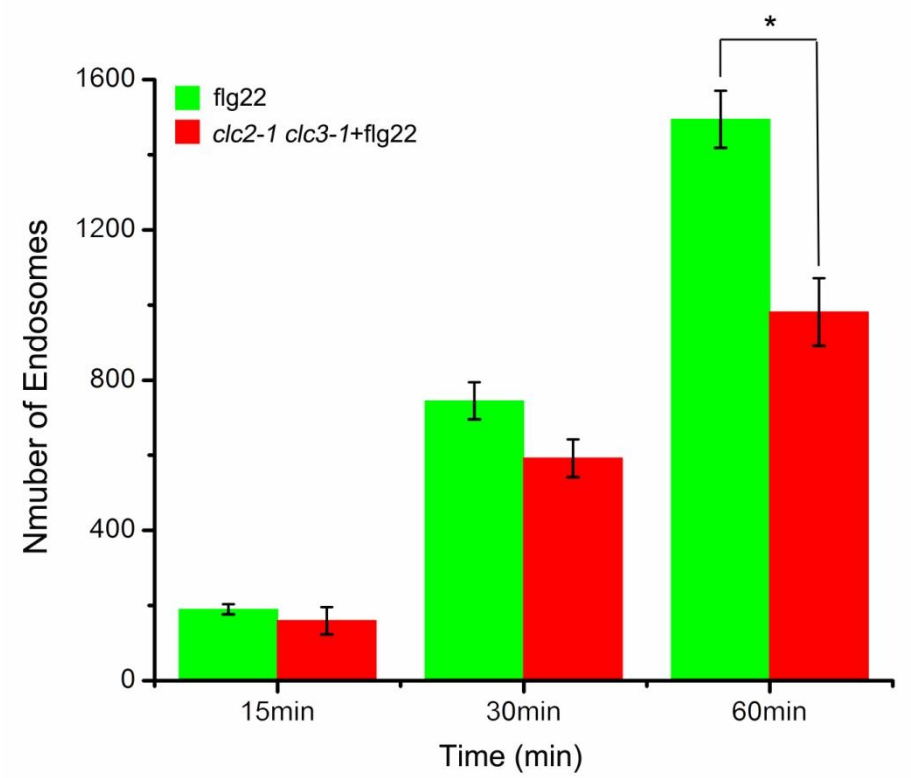

Fig. S8. Clathrin is involved in flg22 induced FLS2 endocytosis.

In *clc2-1 clc3-1* mutant, FLS2-GFP endosome numbers per image area in response to flg22 treatments over time (n = three seedlings for each treatment). Error bars represent the SD. Statistical significance was checked by Student's *t*-test (*P <0.05).

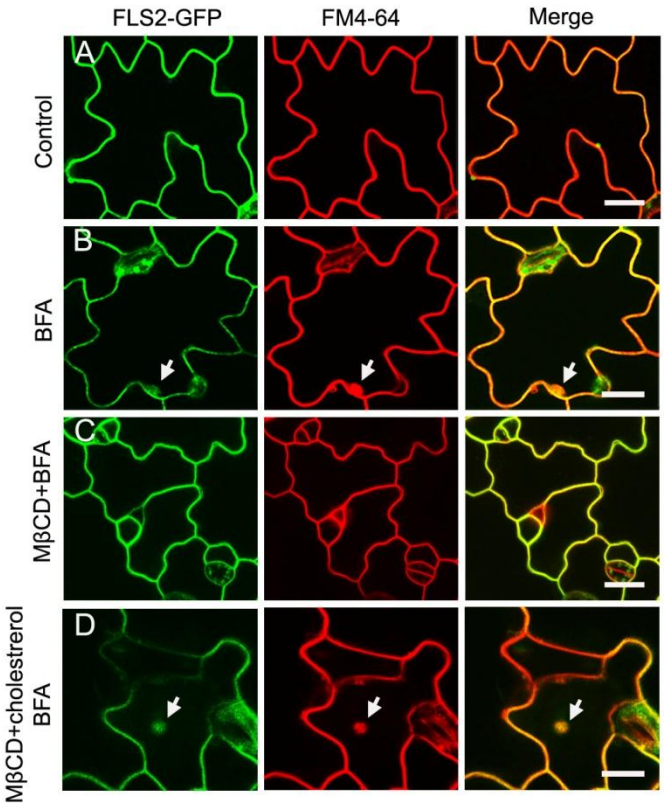

Fig. S9. FLS2-GFP internalization is perturbed by MβCD.

(A) FLS2-GFP co-localized with FM4-64 at the plasma membrane.

(B) FLS2-GFP colocalized with FM4-64 in BFA compartment after BFA treatment.

(C) MβCD reduced the BFA-induced intracellular accumulation of FLS2-GFP.

(D) The effects of sterol complement on FLS2 internalization. Cholesterol was replenished in depleted cells by incubating them with MβCD-cholesterol complexes.

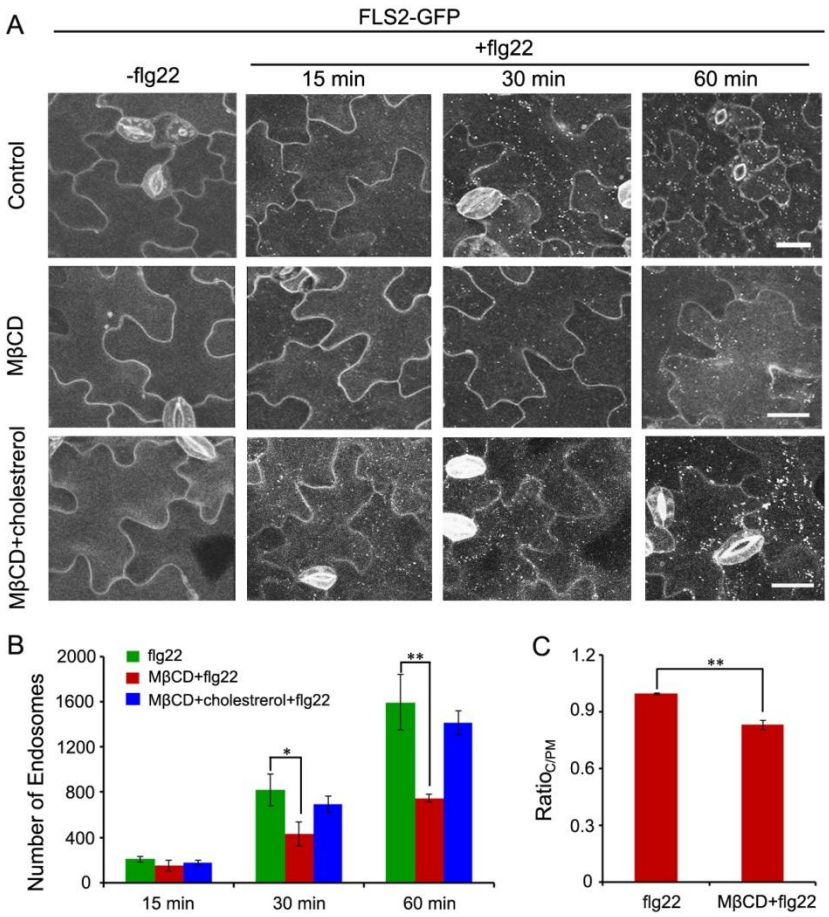

Fig. S10. Sterols are involved in flg22 induced FLS2 endocytosis.

(A) Confocal images of FLS2-GFP treated with flg22, MβCD, MβCD coupled with flg22, or MβCD andMβCD-cholesterol complexes coupled with flg22 co-treatment for 15, 30, and 60 min in *Arabidopsis* leaf epidermis, Bar = 20μm.

(B) FLS2-GFP endosome numbers per image area in response to various treatments over time (n = three seedlings for each treatment). Error bars represent the SD. Statistical significance was checked by Student's *t*-test (*P <0.05 and **P < 0.01).

(C) Quantification of FLS2 endocytosis as estimated by the ratio of the average signal intensity in the cytosol over that at the PM under different conditions (n=33). Error bars represent the SD. Statistical significance was checked by Student's *t*-test (**P < 0.01).

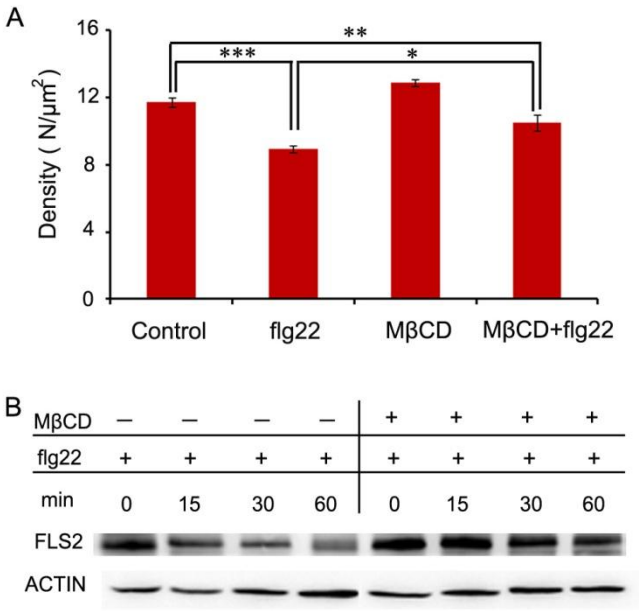

Fig. S11 Sterols are involved in flg22-induced FLS2 degradation.

(A) The density of FLS2-GFP molecules in the different treatments was measured by FCS (n = 30 cells from five seedlings for each treatment). Error bars represent the SD. Statistical significance was checked by Student's *t*-test (*P <0.05, **P < 0.01 and ****P* < 0.001).

(B) Immunoblot analysis of FLS2 protein levels under flg22, flg22 and MβCD co-treatment for 15, 30, and 60 min.

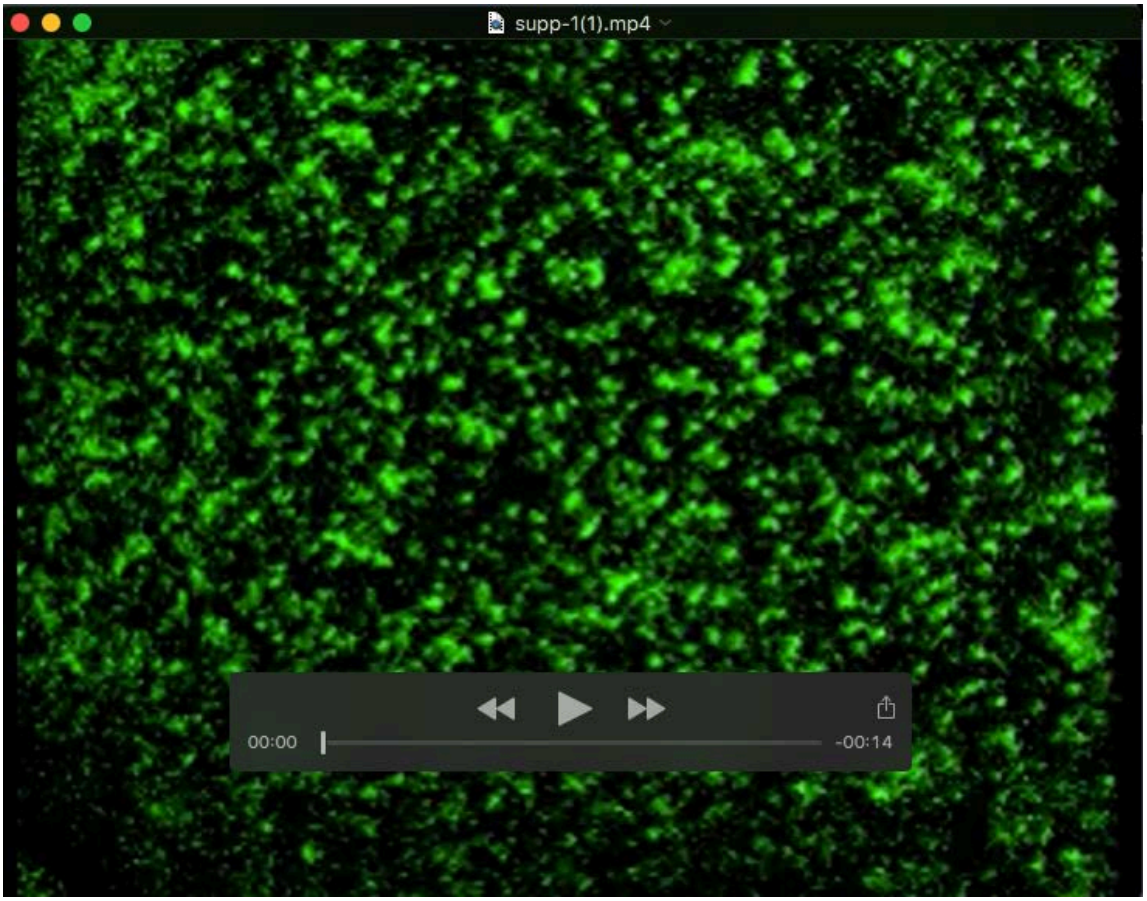

Movie S1. VA-TIRFM imaging of FLS2-GFP spots at the PM of *Arabidopsis* leaves epidermal cells. Movies of 100 frames were acquired; exposure time for each frame was 100 ms.

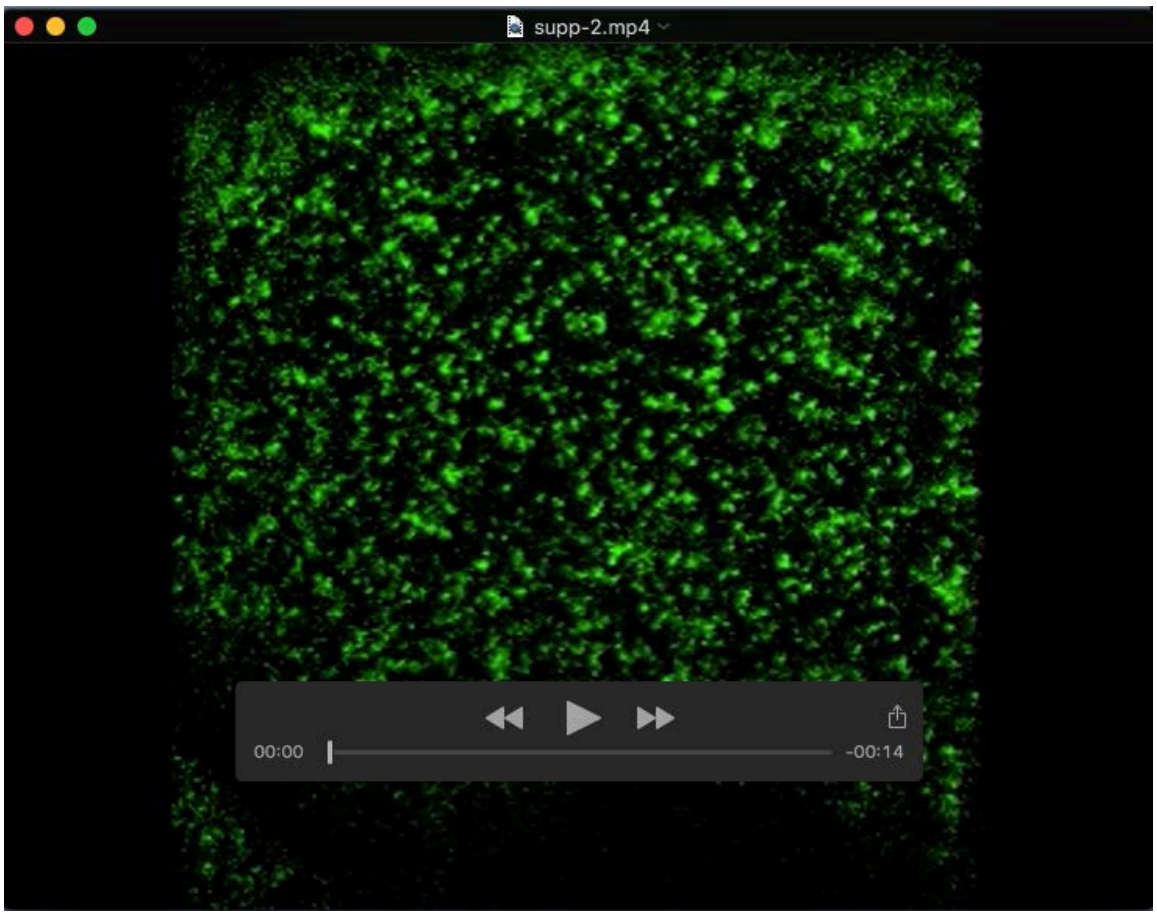

Movie S2. VA-TIRFM imaging of FLS2-GFP spots at the PM of *Arabidopsis* leaves epidermal cells after flg22 treatment. Movies of 100 frames were acquired; exposure time for each frame was 100 ms.

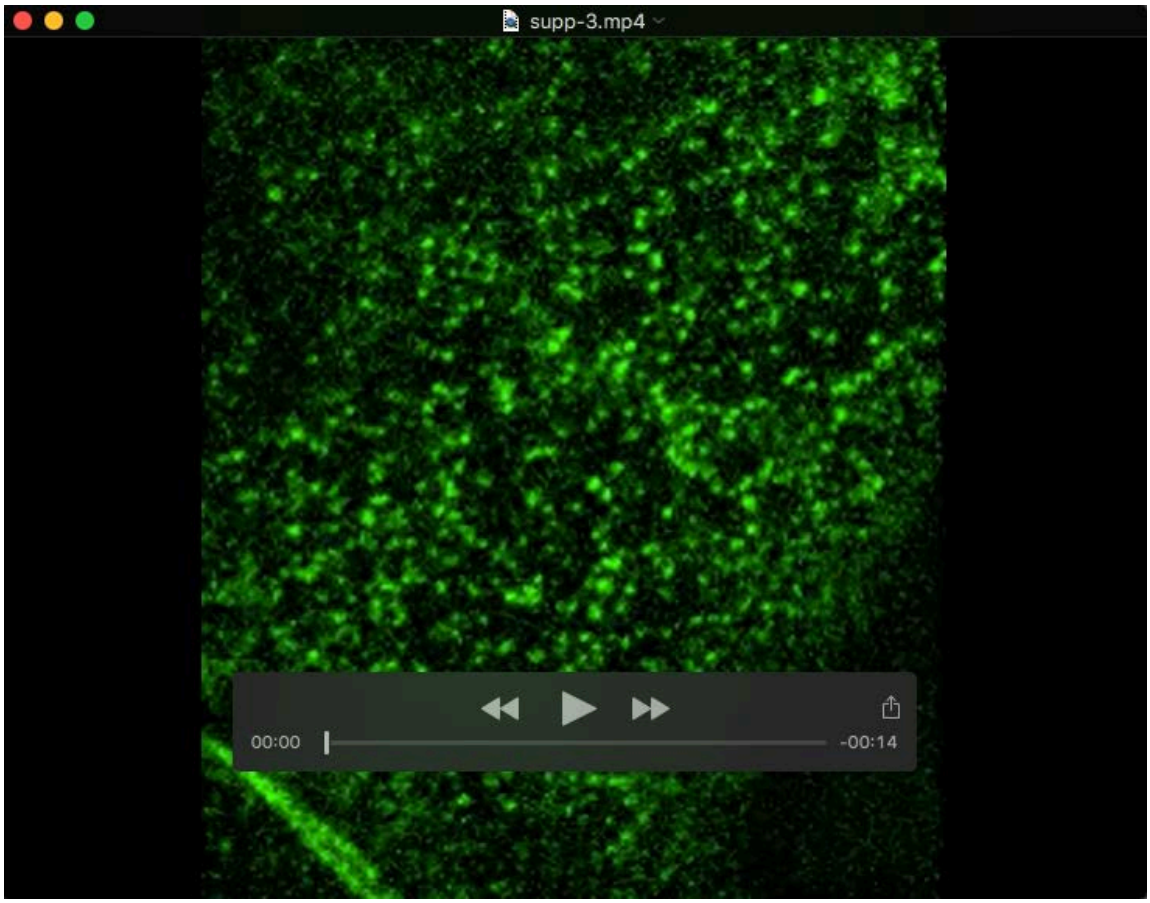

Movie S3. VA-TIRFM imaging of FLS2-GFP spots in *pFLS2*:FLS2-GFP transgenic seedlings in the *smt1* background. Movies of 100 frames were acquired; exposure time for each frame was 100 ms.

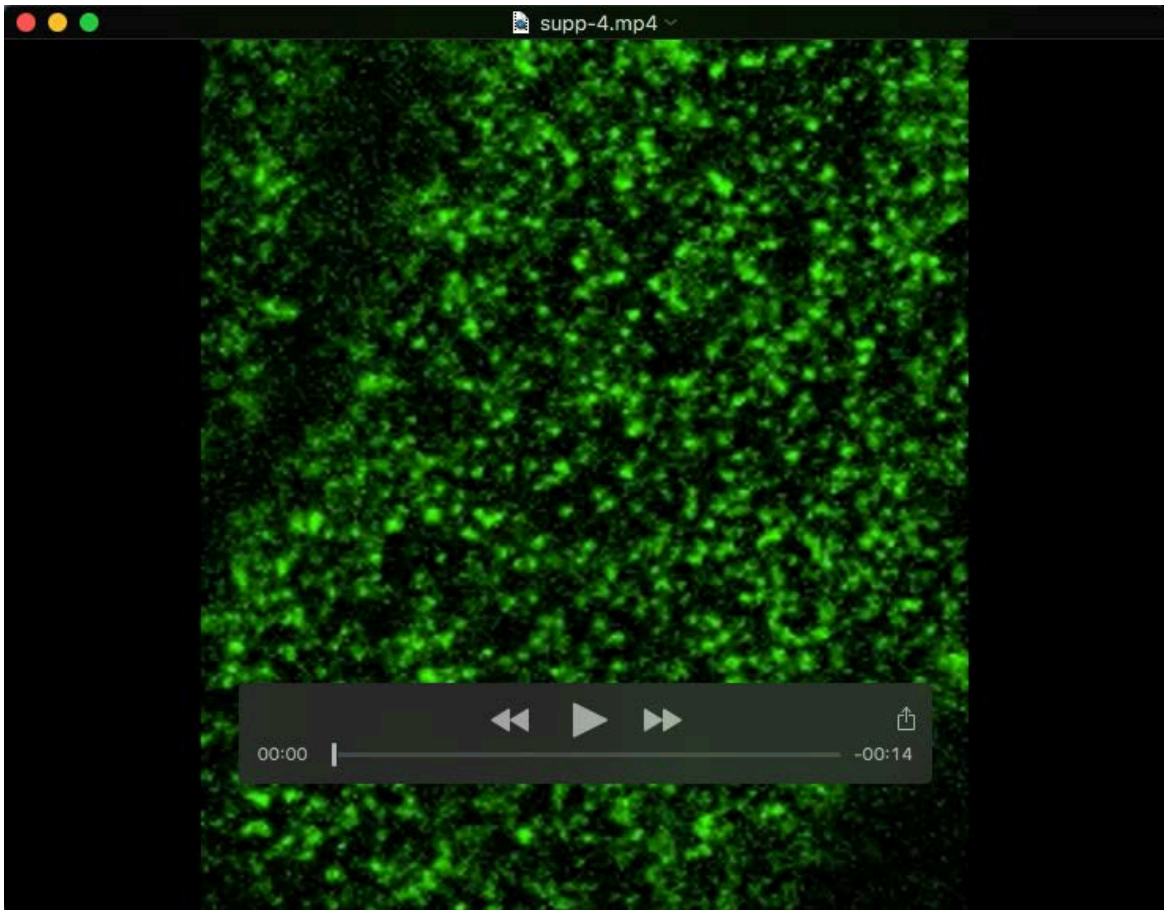

Movie S4. VA-TIRFM imaging of FLS2-GFP spots in *Arabidopsis* leaves epidermal cells treated with 10 mM MβCD. Movies of 100 frames were acquired; exposure time for each frame was 100 ms.